Journal of the European Ceramic Society 41 (2021) 6490–6494

Contents lists available at ScienceDirect

Journal of the European Ceramic Society

journal homepage: www.elsevier.com/locate/jeurceramsoc

Original Article

Structure, chemical bond and microwave dielectric characteristics of novel $Li_3Mg_4NbO_8$ ceramics

Guoguang Yao [a,*], Jiaxin Yan [a], Jingjing Tan [a], Cuijin Pei [a], Peng Liu [b,*], Huaiwu Zhang [c], Dawei Wang [d,*]

[a] School of Science, Xi'an University of Posts and Telecommunications, Xi'an, 710121, China
[b] College of Physics and Information Technology, Shaanxi Normal University, Xi'an, 710062, China
[c] State Key Laboratory of Electronic Thin Films and Integrated Devices, University of Electronic Science and Technology of China, Chengdu, 610054, China
[d] Shenzhen Institute of Advanced Electronic Materials, Shenzhen Institute of Advanced Technology, Chinese Academy of Sciences, Shenzhen, 518055, China

ARTICLE INFO

Keywords:
$Li_3Mg_4NbO_8$ ceramics
Microwave dielectric properties
Orthorhombic structure

ABSTRACT

A novel $Li_3Mg_4NbO_8$ compound was fabricated through the process of solid-state reaction. The crystal structure, sinterability and microwave dielectric properties of the $Li_3Mg_4NbO_8$ ceramics were investigated. XRD refinement and Raman spectra results ascertained that the $Li_3Mg_4NbO_8$ compound crystallized into an orthorhombic $Li_3Mg_2NbO_6$-like structure with space group *Fddd*. The ε_r value was strongly impacted by the relative density and average ionic polarization. The $Q \times f$ value was mainly affected by the relative density and average grain size. The $Li_3Mg_4NbO_8$ ceramics sintered at 1150 ℃ showed outstanding microwave dielectric performance: $\varepsilon_r = 13.8 \pm 0.14$, $Q \times f = 103\ 400 \pm 3500$ GHz (at 9.6 GHz), $\tau_f = -36.0 \pm 1$ ppm/℃. Additionally, the bond characteristics were calculated for a better understanding of the structure-property correlation for $Li_3Mg_4NbO_8$ ceramics.

1. Introduction

As an important member of the functional materials, microwave dielectric materials have been intensively investigated since their intriguing dielectric performance [1]. The development of 5 G to the millimeter wave region has boosted the need for microwave dielectric ceramics with low permittivity (ε_r) [2,3]. Additionally, as considering the practical applications of these materials, it is essential that the candidate dielectric materials have the features of high quality factor ($Q \times f$) as well as near-zero temperature coefficient of resonant frequency (τ_f) value [4–6]. The above three basic characteristics are well known to impact different performance factors of components: (i) low ε_r decreases signal latency, (ii) high $Q \times f$ suppresses signal damping, and (iii) a near-zero τ_f value improves temperature stability. Furthermore, the rapid development of millimeter-wave communication boosts the construction of ultra-large-scale 5 G base stations, new microwave dielectric ceramics with superior performance are urgently explored to address these needs [7–9].

Since the early 1980s, tremendous research has been carried out on the compounds and solid solutions in the Li_2O-MgO-Nb_2O_5 system [10–13]. Two ternary compounds ($Li_3Mg_2NbO_6$, and Li_3MgNbO_5) have been reported. The $Li_3Mg_2NbO_6$-based ceramics have attracted considerable research attention, which is due to their fascinating dielectric and luminescence characteristics [14–23]. Recently, Li et al. firstly reported the crystal structure and dielectric performance ($\varepsilon_r = 16.2$, $Q \times f = 96\ 796$ GHz, τ_f = -24.8 ppm/C) of Li_3MgNbO_5 ceramics [13]. More recently, our group successfully fabricated a new compound of $Li_3Mg_4NbO_8$, which exhibited the same crystal structure as $Li_3Mg_2NbO_6$ [10]. However, the microwave dielectric properties of $Li_3Mg_4NbO_8$ have not been reported so far.

In this work, the microstructure and microwave dielectric properties of $Li_3Mg_4NbO_8$ ceramics were systematically studied. It is well known that microwave dielectric properties are highly dependent on the crystal structure of ceramics, which are particularly explained by the chemical bond theory [24–27]. Therefore, inherent mechanism influencing the microwave dielectric properties of $Li_3Mg_4NbO_8$ ceramics was further investigated based on the Rietveld refinement and complex chemical bond theory.

* Corresponding authors.
E-mail addresses: yaoguoguang@xupt.edu.cn (G. Yao), liupeng@snnu.edu.cn (P. Liu), dw.wang@siat.ac.cn (D. Wang).

https://doi.org/10.1016/j.jeurceramsoc.2021.06.029
Received 22 January 2021; Received in revised form 21 June 2021; Accepted 23 June 2021
Available online 24 June 2021

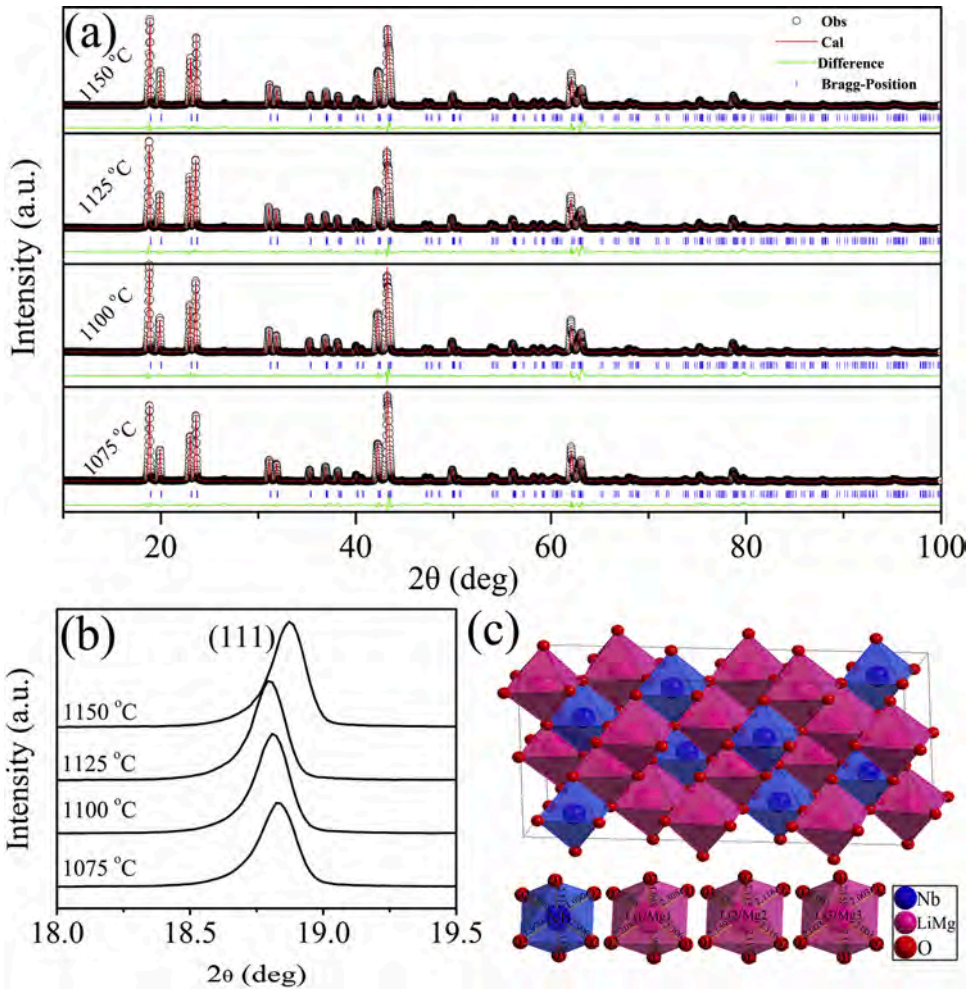

Fig. 1. (a) Rietveld refined XRD patterns, (b) the zoomed (111) peaks for $Li_3Mg_4NbO_8$ ceramics sintered at different temperatures, (c) schematic crystal structure of $Li_3Mg_4NbO_8$.

2. Experimental procedure

$Li_3Mg_4NbO_8$ ceramics was prepared by the conventional solid-state reaction process. Nb_2O_5 (Guo-Yao Co. Ltd., 99.99 %, Shanghai, China), Li_2CO_3 (Guo-Yao Co. Ltd., 98.0 %, Shanghai, China), and MgO (Mountain development center, 99.99 %, Beijing, China) were employed as raw materials. According to formula of $Li_3Mg_4NbO_8$, Li_2CO_3, Nb_2O_5 and MgO were weighed precisely, and then ground for 8 h using zirconia balls and ethanol as grinding media and solvent, respectively. The milled powders were dried in an oven under 80 ℃, calcined under 1000 ℃ for 4 h, and then re-ball milled for 8 h. After drying, the powders were mixed with 5 wt % PVA, granulated and sieved with an 80-mesh screen. The granulated powders were pressed into green discs (Φ10 × 5 mm). After de-binding at 500 ℃ for 2 h, the pellets were sintered at 1075–1175 ℃ for 5 h in air.

The phase structure was identified via the X-ray diffraction (XRD, Smartlab, Japan), using Cu*Ka1* radiation under the condition of 40 kV and 100 mA. The specimens were scanned in the range of 10−100°, with a step size of 0.01° and a count time of 2 s. Rietveld refinement of the XRD data was undertaken by the GSAS-EXPGUI software [28]. The cross-sections of the sintered samples were ground using abrasive papers and polished with a 2.5 μm diamond spray polishing agent, followed by a thermal etching at temperatures 100 °C below the sintering temperatures. The microstructure was examined by a scanning electron microscopy (SEM, Hitachi, Tokyo, Japan), and the average grain size was calculated using the image analysis software (Nano Measurer 1.2). Ambient Raman spectra (100−1000 cm^{-1}) were collected using a Raman spectrometer (Jobin Yvon, Longjumeau, France) equipped with a He-Ne laser (514 nm) and an output of 30 mW, and the peak positions were analyzed by a Peakfit Demo software. Archimedes' principle was carried out to determine the bulk densities. The ε_r and Q × f values of samples were tested using a Rohde & Schwarz ZVB20 vector network analyzer under 9.0–10.0 GHz by the $TE_{01}\delta$ mode using a cavity. The τ_f value for samples was calculated by the following formula:

Table 1
Refinement parameters, reliability factors, and ρ_{theo} of $Li_3Mg_4NbO_8$ ceramics with different sintering temperatures.

T (°C)	a (Å)	b (Å)	c (Å)	cell volume (Å^3)	ρ_{theo}(g/cm^3)	Rp(%)	Rwp(%)
1075	5.8993(5)	8.5427(6)	17.7262(1)	893.3280(3)	3.782	8.90	13.27
1100	5.8997(5)	8.5441(7)	17.7368(1)	894.0801(4)	3.779	9.54	14.31
1125	5.9017(5)	8.5452(7)	17.7385(1)	894.5891(4)	3.777	9.15	13.83
1150	5.8962(2)	8.5390(2)	17.7260(5)	892.4578(3)	3.786	9.51	14.70

T: sintering temperature; R_{wp}: the reliability factor of weighted patterns; R_p: the reliability factor of patterns.

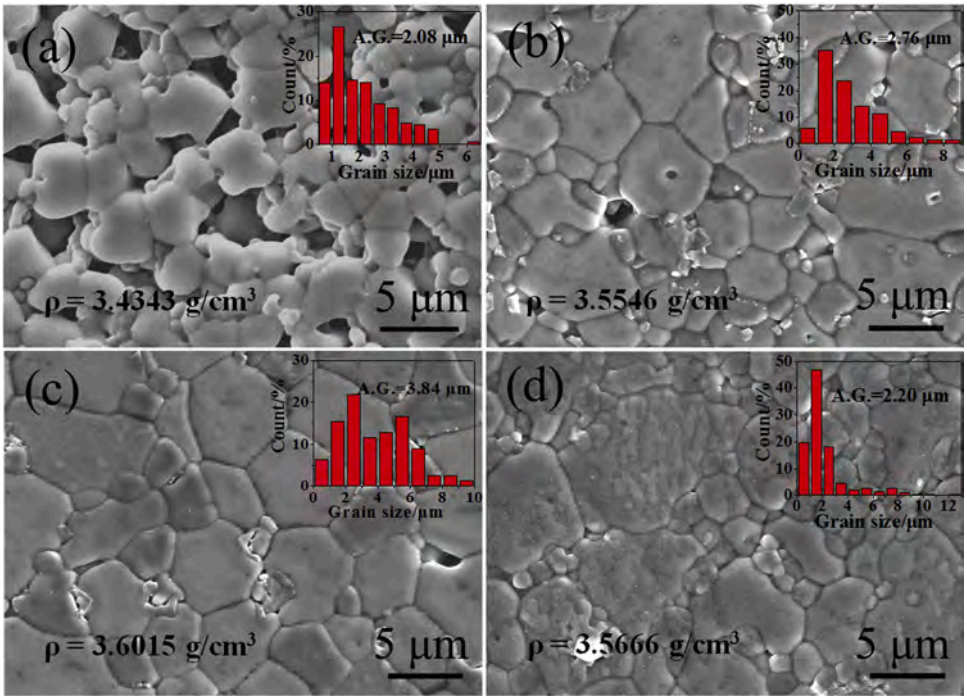

Fig. 2. Typical SEM micrographs, grain size distribution and bulk density of $Li_3Mg_4NbO_8$ sintered at different temperatures: (a) 1075 ℃, (b) 1100 ℃, (c) 1150 ℃, (d) 1175 ℃.

$$\tau_f = \frac{(f_2 - f_1) \times 10^6}{f_1 \times (80 - 20)} \quad (1)$$

in which f_1 and f_2 is the resonant frequency measured at 20 ℃ and 80 ℃.

3. Results and discussion

Fig. 1(a) displays the Rietveld refined XRD patterns of the $Li_3Mg_4NbO_8$ ceramics sintered at different temperatures, the corresponding refined results are listed in Table 1. Rietveld refinement has been carried out based on an orthorhombic $Li_3Mg_2NbO_6$ structure (JCPDS 86-0346) as the initial model and yielded in good fits. As shown in Fig. 1(a), the diffraction peaks for all specimens matched well with the standard pattern of $Li_3Mg_2NbO_6$, indicating that $Li_3Mg_4NbO_8$ belongs to the orthorhombic structure with a *Fddd* space group. As illustrated in Fig. 1(b), the main diffraction peak (111) initially shifted towards a lower angle and then to a higher angle with the increase of sintering temperature. The main diffraction peak (111) is relevant to the long-range ordering as reported by Tang et al. [22]. The schematic crystal structure of the $Li_3Mg_4NbO_8$ compound is shown in Fig. 1(c), which exhibits a partially ordered rock salt superstructure with six formula units per unit cell, where Nb atoms locate at 8a and Li/Mg atoms locate at 8b and 16 g Wyckoff sites separately. There are four types of oxygen octahedra in $Li_3Mg_4NbO_8$, and the isolated NbO_6 ordering octahedra share edges with 12 adjacent $(Li/Mg)O_6$ partially ordering octahedra [12]. Table 1 lists the refinement parameters of the $Li_3Mg_4NbO_8$ ceramics under various sintering temperatures. Note that all the Rp and Rwp values were lower than 15 % and Rp < Rwp, indicating that the obtained refinement data were reliable. As observed in Table 1, the lattice parameters and cell volume increased firstly and then decreased, which confirmed the above shift of the diffraction peak (111).

Fig. 2 presents the typical SEM micrographs of polished and thermal etched cross-sections of $Li_3Mg_4NbO_8$ samples sintered at different temperatures. The average grain size and bulk density are given in the insets of Fig. 2. The average grain size increased from ~2.76 μm to ~3.84 μm with increasing sintering temperature from 1075 ℃ to 1150 ℃, and then decreased to ~2.20 μm for sample sintered at 1175 ℃. For specimen sintered at 1150 ℃, a dense and uniform microstructure was achieved, as seen in Fig. 2(c). However, partial melting of grains along with uneven microstructure was observed due to the over-sintering at high temperature, leading to the decline of bulk density, as shown in Fig. 2 (d).

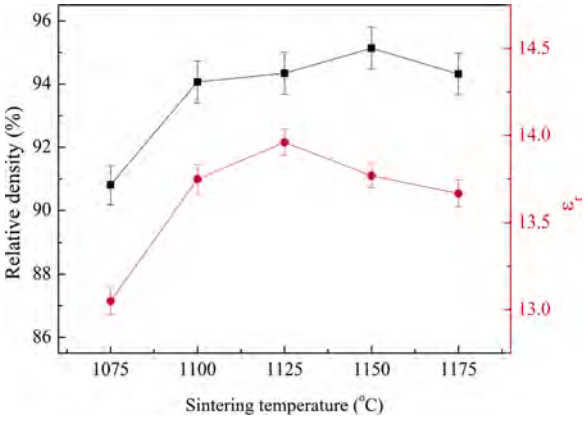

Fig. 3. Changes in relative density and ε_r of $Li_3Mg_4NbO_8$ ceramics as a function of sintering temperature.

The relative density and ε_r for $Li_3Mg_4NbO_8$ ceramics as a function of sintering temperature are shown in Fig. 3. With the increase of sintering temperature, the relative density was found to increase rapidly, which achieved its maximum value at 1150 ℃ and descended slightly thereafter, in consistence with the microstructure (Fig. 2). It is well known that the ε_r of single-phase ceramics is mainly dominated by the relative density and average ionic polarization (α_{theo}/V_m) [29]. As shown in Fig. 3, with the increase of sintering temperature, the ε_r firstly increased from 13.1 ± 0.15 to the maximum value of 14.0 ± 0.13 and then decreased to 13.7 ± 0.15. The improvement in ε_r of $Li_3Mg_4NbO_8$ ceramics could be attributed to the enhancement in relative density, while

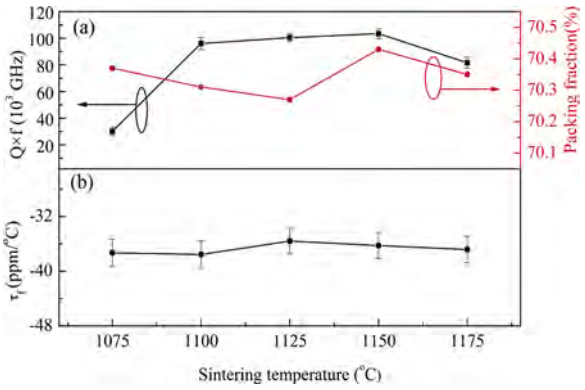

Fig. 4. Changes in Q × f, and τ_f of $Li_3Mg_4NbO_8$ ceramics as a function of sintering temperature.

the decrease in ε_r could be attributed to the integrated factors of the relative density and the decreased α_{theo}/V_m caused by lithium volatilization during high temperature sintering process [30,31]. Furthermore, the corrected dielectric constant (ε_{corr}) of 14.4 was calculated using the formula $\varepsilon_{corr} = \varepsilon_r(1 + 1.5p)$ (p denotes the fractional porosity) to exclude the influence of porosity for $Li_3Mg_4NbO_8$ ceramics sintered at 1150 ℃. The theoretical dielectric constant (ε_{th}) of 14.2 was also calculated by the Clausius-Mosotti equation [32]. The ε_{corr} value (14.4) was comparable to the ε_{th} value (14.2), and the deviation between them was less than 1.5 %.

The temperature-dependent Q × f and τ_f for $Li_3Mg_4NbO_8$ ceramics are shown in Fig. 4. Generally, both external (density, defect, impurity, etc.) and internal factors (vibration modes and packing fraction) have significant influence on the Q × f value of ceramics [33,34]. Kim et al. found that Q × f was positively correlated with packing fraction of ceramics, which was due to that a high packing fraction corresponded to a weak lattice vibration and thus a low loss [35]. As shown in Fig. 4(a), there was no positive correlation between the packing fraction and Q × f value, especially for the samples sintered below 1150 ℃, suggesting that the packing fraction was not the key factor influencing the Q × f value. Lowndes et al. found that relative density significantly affected Q × f of ceramics with single phase, because of the modified lattice vibrations result from the presence of pores [36]. As presented in Fig. 4(a), with the increase of sintering temperature from 1075 ℃ to 1150 ℃, the Q × f value firstly increased from 30 200 ± 3000 GHz to the maximum value of 103 400 ± 3500 GHz, and then decreased to 81 600 ± 4100 GHz with further increasing sintering temperature to 1175 ℃. Here, the variation in Q × f with sintering temperature was consistent with the fact of the relative density and average grain size, indicating that the Q × f value of samples was mainly determined by the relative density and average grain size [37]. Additionally, the data provided in Fig. 4(b) indicated that τ_f remained stable at around -36.0 ± 1 ppm/℃ at different sintering temperatures, which was attributed to the unchanged crystal structure as shown in XRD patterns and Raman spectra [38].

The chemical bond parameters associated with the Phillips-Van-Levine (P-V-L) chemical bond theory have been proved to be critical for impacting microwave dielectric properties [39–42]. Thus, specific chemical bond parameters (bond ionicity, bond energy and lattice energy) of $Li_3Mg_4NbO_8$ ceramics were evaluated based on the P-V-L theory. The complex $Li_3Mg_4NbO_8$ crystals were at first decomposed into binary crystals according to the detailed structure information and the P-V-L theory:

Table 2
The average bond ionicity (Af_i), average lattice energy (AU_b) and average bond energy (AE_b) of $Li_3Mg_4NbO_8$ ceramics sintered at 1150 ℃.

Bond type	Af_i	AU_b (kJ/mol)	AE_b (kJ/mol)
Nb—O	89 %	10722.69	567.31
Li—O	61 %	401.28	392.50
Mg—O	75 %	2213.84	278.05

$$\begin{aligned} Li_3Mg_4NbO_8 &= Li(1)Li(2)Li(3)Mg(1)_{4/3}Mg(2)_{4/3}Mg(3)_{4/3}NbO(1)_{8/3}O(2)_{16/3} \\ &= Li(1)_{1/3}O(1)_{4/9} + Li(1)_{1/3}O(2)^1_{4/9} + Li(1)_{1/3}O(2)^2_{4/9} \\ &\quad + Li(2)_{1/3}O(1)_{4/9} + Li(2)_{1/3}O(2)^1_{4/9} + Li(2)_{1/3}O(2)^2_{4/9} \\ &\quad + Li(3)_{1/3}O(1)_{2/9} + Li(3)_{2/3}O(2)_{4/9} + Mg(1)_{4/9}O(1)_{4/9} \\ &\quad + Mg(1)_{4/9}O(2)^1_{4/9} + Mg(1)_{4/9}O(2)^2_{4/9} + Mg(2)_{4/9}O(1)_{4/9} \\ &\quad + Mg(2)_{4/9}O(2)^1_{4/9} + Mg(2)_{4/9}O(2)^2_{4/9} + Mg(3)_{4/9}O(1)_{2/9} \\ &\quad + Mg(3)_{8/9}O(2)_{4/9} + Nb_{1/3}O(1)_{4/9} + Nb_{2/3}O(2)_{8/9} \end{aligned} \quad (2)$$

The detailed calculation process for determining chemical bond parameters has been described previously [23,42]. Tables S1-S2 list the detailed bond ionicity, bond energy and lattice energy of $Li_3Mg_4NbO_8$ ceramics sintered at 1150 ℃, respectively. It was reported that the ε_r was positively correlated with the bond ionicity (f_i) based on the formula (3).

$$\varepsilon_r = \frac{n^2 - 1}{1 - f_i} + 1 \quad (3)$$

According to Zhang et al., the high lattice energy corresponded to the high stability of the ionic crystal, and thus a high Q×f value [43]. As shown in Table 2, average bond ionicity (Af_i) and average lattice energy (AU_b) exhibited the same sequence: Af_i(Li-O) < Af_i (Mg-O) < Af_i (Nb-O) and AU_b(Li-O) < AU_b(Mg-O) < AU_b (Nb-O), suggesting that the Nb-O bond had an important effect on the ε_r, Q × f of $Li_3Mg_4NbO_8$ ceramics. The same conclusion was also reported in $Li_3Mg_2NbO_6$ ceramics [19,21]. Furthermore, the bond energy, indicating the stability of the crystal structure, was intimately linked to τ_f value [44]. As seen in Table 2, the average bond energy of Nb-O bond (567.31 kJ/mol) was much higher than that of Li-O (392.50 kJ/mol) and Mg-O (278.05 kJ/mol) bonds, indicating that the Nb-O bond served a vital function in the resulting τ_f value of $Li_3Mg_4NbO_8$ ceramics, which agreed to the result in Ta^{5+} substituted $Li_3Mg_2NbO_6$ ceramics [45].

4. Conclusions

Novel $Li_3Mg_4NbO_8$ ceramics were successfully fabricated by a solid-state reaction route. The $Li_3Mg_4NbO_8$ compounds crystallized in an orthorhombic structure with a space group of *Fddd*. Dense $Li_3Mg_4NbO_8$ ceramics were obtained at 1150 ℃. The ε_r value was determined by the combined effects of the relative density and average ionic polarization. The Q × f value was closely related to the relative density and microstructure. The $Li_3Mg_4NbO_8$ ceramics sintered at 1150 ℃ displayed good microwave dielectric performance of ε_r = 13.8 ± 0.14, Q × f = 103 400 ± 3500 GHz (at 9.6 GHz), τ_f = -36.0 ± 1 ppm/℃. P—V—L bond theory analysis indicated that the intrinsic microwave dielectric properties of $Li_3Mg_4NbO_8$ ceramics were highly dependent on the Nb—O bond.

Declaration of Competing Interest

The authors declare that they have no known competing financial interests or personal relationships that could have appeared to influence the work reported in this paper.

Acknowledgements

The authors acknowledge supports from National Natural Science Foundation of China (Grant No 52002317), Shaanxi Province Natural Science Foundation, China (Grant No. 2021JM-458) and Xi'an Science and technology Bureau (GXYD17.19).

Appendix A. Supplementary data

Supplementary material related to this article can be found, in the online version, at doi:https://doi.org/10.1016/j.jeurceramsoc.2021.06.029.

References

[1] L.Y. Ao, Y. Tang, J. Li, W.S. Fang, L. Duan, C.X. Su, Y.H. Sun, L.J. Liu, L. Fang, Structure characterization and microwave dielectric properties of $LiGa_5O_8$ ceramic with low-ε_r and low loss, J. Eur. Ceram. Soc. 40 (2020) 5498–5503.
[2] Y.F. Zhai, Y. Tang, J. Li, L. Duan, C.X. Su, A. Cao, C.Y. Jin, L. Fang, Structure, Raman spectra and properties of two low-ε_r microwave dielectric ceramics $Ca_3B_2Ge_3O_{12}$ (B = Al, Ga), Ceram. Int. 46 (2020) 28710–28715.
[3] J.J. Zheng, Y.K. Yang, H.T. Wu, Y.Y. Zhou, Z.L. Zhang, Structure, infrared spectra and microwave dielectric properties of the novel Eu_2TiO_5 ceramics, J. Am. Ceram. Soc. 103 (2020) 4333–4341.
[4] Y. Tang, Z.W. Zhang, J. Li, M.Y. Xu, Y.F. Zhai, L. Duan, C.X. Su, L.J. Liu, Y.H. Sun, L. Fang, $A_3Y_2Ge_3O_{12}$ (A = Ca, Mg): two novel microwave dielectric ceramics with contrasting τ_f and Q×f, J. Eur. Ceram. Soc. 40 (2020) 3988–3995.
[5] X.Q. Song, W.Z. Lu, Y.H. Lou, T. Chen, S.W. Tac, Z.X. Fu, W. Lei, Synthesis, lattice energy and microwave dielectric properties of $BaCu_{2-x}Co_xSi_2O_7$ ceramics, J. Eur. Ceram. Soc. 40 (2020) 3035–3041.
[6] J. Krupka, P.G. Shakhil, N.S. Arun, R. Ratheesh, H. Jantunen, H.T. Kim, M. T. Sebastian, Low loss polypropylene-silicon composites for millimetre wave applications, Mater. Res. Bull. 104 (2018) 143–148.
[7] J. Li, Y. Tang, Z.W. Zhang, W.S. Fang, L.Y. Ao, A.H. Yang, L.J. Liu, L. Fang, Two novel garnet $Sr_3B_2Ge_3O_{12}$ (B = Yb, Ho) microwave dielectric ceramics with low permittivity and high Q, J. Eur. Ceram. Soc. 41 (2021) 1317–13023.
[8] X.Q. Chen, H. Li, P.C. Zhang, G.S. Li, Microwave dielectric properties of $Co_2P_2O_7$ ceramics, Ceram. Int. 47 (2021) 1980–1985.
[9] D. Szwagierczak, B. Synkiewicz-Musialska, J. Kulawik, E. Czerwinska, N. Pałka, P. R. Bajurko, Low temperature sintering of $Zn_4B_6O_{13}$ based substrates, their microstructure and dielectric properties up to the THz range, J. Alloys Compd. 819 (2020), 153025.
[10] M. Castellanos, J.A. Gard, A.R. West, Crystal data for a new family of phases, $Li_3Mg_2XO_6$: x=Nb, Ta, Sb, J. Appl. Cryst. 15 (1982) 116–119.
[11] L.L. Yuan, J.J. Bian, Microwave dielectric properties of the lithium containing compounds with rock salt structure, Ferroelectrics 387 (2009) 123–129.
[12] J.J. Bian, Z. Liang, L. Wang, Structural evolution and microwave dielectric properties of $Li_{3-3x}M_{4x}Nb_{1-x}O_4$ (M=Mg,Zn; $0 \le x \le 0.9$), J. Am. Ceram. Soc. 94 (2011) 1447–1453.
[13] J. Li, Z.W. Zhang, Y.F. Tian, L.Y. Ao, J.Q. Chen, C.X. Su, L.J. Liu, Y. Tang, L. Fang, Crystal structure and microwave dielectric properties of a novel rock-salt type Li_3MgNbO_5 ceramic, J. Mater. Sci. 55 (2020) 15643–15652.
[14] X.C. Wang, X.P. Zhou, Y.X. Cao, Q. Wei, Z.Y. Zhao, Y.H. Wang, Insight into a novel rare-earth-free red-emitting phosphor $Li_3Mg_2NbO_6:Mn^{4+}$: structure and luminescence properties, J. Am. Ceram. Soc. 102 (2019) 6724–6731.
[15] P. Zhang, M.M. Hao, M. Xiao, Microwave dielectric properties of $Li_3Mg_2NbO_6$-based ceramics with $(M_xW_{1-x})^{5+}$(M = Li^+, Mg^{2+}, Al^{3+}, Ti^{4+}) substitutions at Nb^{5+}sites, J. Alloys Compd. 853 (2021), 157386.
[16] X. Zhang, X. Zhang, Z.X. Fang, Z. Xiong, H.Y. Yang, S.R. Zhang, B. Tang, Effects of lattice evolution and ordering on the microwave dielectric properties of Tin-modified $Li_3Mg_2NbO_6$-based ceramics, J. Phys. Chem. 124 (2020) 22069–22081.
[17] T.W. Zhang, R.Z. Zuo, Effect of Li_2O-V_2O_5 addition on the sintering behavior and microwave dielectric properties of $Li_3(Mg_{1-x}Zn_x)_2NbO_6$ ceramics, Ceram. Int. 40 (2014) 15677–156841.
[18] P. Zhang, K.X. Sun, X.R. Mao, M. Xiao, Z.T. Zheng, Crystal structures and high microwave dielectric properties in Li^+/Ti^{4+} ions co-doped $Li_3Mg_2NbO_6$ ceramics, Ceram. Int. 46 (2020) 8097–8103.
[19] H.T. Wu, E.S. Kim, Characterization of low loss microwave dielectric materials $Li_3Mg_2NbO_6$ based on the chemical bond theory, J. Alloys Compd. 669 (2016) 134–140.
[20] P. Zhang, K. Sun, M. Xiao, Z. Zheng, Crystal structure, densification, and microwave dielectric properties of $Li_3Mg_2(Nb_{(1-x)}Mo_x)O_{6+x/2}$ ($0 \le x \le 0.08$) ceramics, J. Am. Ceram. Soc. 102 (2019) 4127–4135.
[21] P. Zhang, S. Wu, M. Xiao, Effect of Sb^{5+} ion substitution for Nb^{5+} on crystal structure and microwave dielectric properties for $Li_3Mg_2NbO_6$ ceramics, J. Alloys Compd. 766 (2018) 498–505.
[22] X. Zhang, B. Tang, Z. Fang, H. Yang, Z. Xiong, L. Xue, S. Zhang, Structural evolution and microwave dielectric properties of a novel $Li_3Mg_{2-x/3}Nb_{1-2x/3}Ti_xO_6$ system with a rock salt structure, Inorg. Chem. Front. 5 (2018) 3113–3125.
[23] W.S. Xia, L.X. Li, P.F. Ning, Q.W. Liao, Relationship between bond ionicity, lattice energy, and microwave dielectric properties of $Zn(Ta_{1-x}Nb_x)_2O_6$ Ceramics, J. Am. Ceram. Soc. 95 (2012) 2587–2592.
[24] H.Y. Yang, S.R. Zhang, H.C. Yang, E.Z. Li, Usage of P-V-L bond theory in studying the structural/property regulation of microwave dielectric ceramics: a review, Inorg. Chem. Front. 7 (2020) 4711–4753.
[25] Y. Zhang, S.H. Ding, C. Li, T.X. Song, Y.C. Zhang, Bond analysis of novel $MnZrTa_2O_8$ microwave dielectric ceramics with monoclinic structure, J. Mater. Sci. 55 (2020) 8491–8501.
[26] B.W. Zhang, L.X. Li, W.J. Luo, Oxygen vacancy regulation and its high frequency response mechanism in microwave ceramics, J. Mater. Chem. C 6 (2018) 11023–11034.
[27] E. Kroumova, M.I. Aroyo, J.M. Perez-Mato, A. Kirov, C. Capillas, S. Ivantchev, H. Wondratschek, Bilbao crystallographic server: Useful databases and tools for phase-transition studies, Phase Transit. 76 (2003) 155–170.
[28] A.C. Larson, R.B. Von Dreele, General structure analysis system (GSAS), in: Los Alamos National Laboratory Report LAUR, 86, 2004.
[29] M.K. Du, L.X. Li, S.H. Yu, Z. Sun, J.L. Qiao, High-Q microwave ceramics of Li_2TiO_3 co-doped with magnesium and niobium, J. Am. Ceram. Soc. 101 (2018) 4066–4075.
[30] G.G. Yao, C.J. Pei, P. Liu, H.Y. Xing, L.X. Fu, B.C. Liang, Novel temperature stable $Ba_{1-x}Sr_xV_2O_6$ microwave dielectric ceramics with ultra-low sintering temperature, J. Mater. Sci-Mater. El. 28 (2017) 13283–13288.
[31] J.Z. Gong, H.F. Zhou, F. He, X.L. Chen, J. Chen, L. Fang, Structural evolution, low-firing characteristic and microwave dielectric properties of magnesium and sodium vanadate ceramic, Ceram. Int. 41 (2015) 11125–11131.
[32] E.R. Kipkoech, F. Azough, R. Freer, Microstructural control of microwave dielectric properties in $CaTiO_3$-$La(Mg_{1/2}Ti_{1/2})O_3$ ceramics, J. Appl. Phys. 97 (2005), 064103.
[33] V.L. Gurevich, A.K. Tagantsev, Intrinsic dielectric loss in crystals, Adv. Phys. 40 (1991) 719–767.
[34] K.G. Wang, H.F. Zhou, X.B. Liu, W.D. Sun, X.L. Chen, H. Ruan, A lithium aluminium borate composite microwave dielectric ceramic with low permittivity, near-zero shrinkage, and low sintering temperature, J. Eur. Ceram. Soc. 39 (2019) 1122–1126.
[35] E.S. Kim, C.J. Jeon, P.G. Clem, Effects of crystal structure on the microwave dielectric properties of ABO_4 (A = Ni, Mg, Zn and B = Mo, W) ceramics, J. Am. Ceram. Soc. 95 (2012) 2934–2938.
[36] R. Lowndes, F. Azough, R. Cernik, R. Freer, Structures and microwave dielectric properties of $Ca_{(1-x)}Nd_{2x/3}TiO_3$ ceramics, J. Eur. Ceram. Soc. 32 (2012) 3791–3799.
[37] S.J. Penn, N.M. Alford, A. Templeton, X.R. Wang, M.S. Xu, M. Reece, K. Schrapel, Effect of porosity and grain size on the microwave dielectric properties of sintered Alumina, J. Am. Ceram. Soc. 80 (1997) 1885–1888.
[38] M. Parastoo, T.N. Ehsan, T.A. Hamid, Effect of Zinc ions non-stoichiometry on the microstructure and microwave dielectric properties of $Li_2ZnTi_3O_8$ ceramics, J. Alloys Compd. 695 (2017) 3772–3778.
[39] J.C. Phillips, Ionicity of the chemical bond in crystals, Rev. Modern. Phys. 42 (1970) 317–356.
[40] J.A. Van Vechten, Quantum dielectric theory of electronegativity in covalent systems. II. Ionization potentials and interband transition energies, Phys. Rev. 187 (1969) 1007–1020.
[41] B.F. Levine, Bond susceptibilities and ionicities in complex crystal structures, J. Chem. Phys. 59 (1973) 1463–1486.
[42] Z.J. Wu, S.Y. Zhang, Semiempirical method for the evaluation of bond covalency in complex crystals, J. Phys. Chem. A 103 (1999) 4270–4274.
[43] P. Zhang, Y.G. Zhao, Effects of structural characteristics on microwave dielectric properties of $Li_2Mg(Ti_{1-x}Mn_x)_3O_8$ ceramics, J. Alloys Compd. 647 (2015) 386–391.
[44] A.M. Glazer, The classification of tilted octahedral perovskites, Acta. Crystallogr. B 28 (1972) 3384–3392.
[45] G. Wang, D.N. Zhang, H.W. Zhang, Crystal structure and enhanced microwave dielectric properties of Ta^{5+} substituted $Li_3Mg_2NbO_6$ ceramics, J. Am. Ceram. Soc. 40 (2020) 3035–3041.